

A novel multistep mechanism for initial lymphangiogenesis in mouse embryos based on ultramicroscopy

René Hägerling^{1,7}, Cathrin Pollmann^{1,7}, Martin Andreas¹, Christian Schmidt¹, Harri Nurmi², Ralf H Adams³, Kari Alitalo², Volker Andresen⁴, Stefan Schulte-Merker^{5,6} and Friedemann Kiefer^{1,*}

¹Mammalian Cell Signaling Laboratory, Department of Vascular Cell Biology, Max Planck Institute for Molecular Biomedicine, Münster, Germany, ²Molecular/Cancer Biology Laboratory, Biomedicum Helsinki, University of Helsinki, Helsinki, Finland, ³Department of Tissue Morphogenesis, Faculty of Medicine, Max Planck Institute for Molecular Biomedicine, University of Münster, Münster, Germany, ⁴LaVision BioTec GmbH, Bielefeld, Germany, ⁵Developmental Biology, Hubrecht Institute, CT Utrecht, The Netherlands and ⁶EZO, University of Wageningen, The Netherlands

During mammalian development, a subpopulation of endothelial cells in the cardinal vein (CV) expresses lymphatic-specific genes and subsequently develops into the first lymphatic structures, collectively termed as lymph sacs. Budding, sprouting and ballooning of lymphatic endothelial cells (LECs) have been proposed to underlie the emergence of LECs from the CV, but the exact mechanisms of lymph vessel formation remain poorly understood. Applying selective plane illumination-based ultramicroscopy to entire wholemount-immunostained mouse embryos, we visualized the complete developing vascular system with cellular resolution. Here, we report emergence of the earliest detectable LECs as strings of loosely connected cells between the CV and superficial venous plexus. Subsequent aggregation of LECs resulted in formation of two distinct, previously unidentified lymphatic structures, the dorsal peripheral longitudinal lymphatic vessel (PLLV) and the ventral primordial thoracic duct (pTD), which at later stages formed a direct contact with the CV. Providing new insights into their function, we found vascular endothelial growth factor C (VEGF-C) and the matrix component CCBE1 indispensable for LEC budding and migration. Altogether, we present a significantly more detailed view and novel model of early lymphatic development.

The EMBO Journal (2013) **32**, 629–644. doi:10.1038/emboj.2012.340; Published online 8 January 2013

Subject Categories: development

Keywords: lymph vessel development; ultramicroscopy; VEGFR-3; CCBE1; VEGF-C

*Corresponding author. Department of Vascular Cell Biology, Max Planck Institute for Molecular Biomedicine, Röntgenstrasse 20, 48149 Münster, Germany. Tel.: +49 251 70365 230; Fax: +49 251 70365 297; E-mail: fkiefer@gwdg.de

⁷These authors contributed equally to this work.

Received: 3 May 2012; accepted: 5 December 2012; published online: 8 January 2013

Introduction

Lymphatic vessels, the second vascular system of vertebrates, are indispensable for tissue homeostasis. The lymphatic vasculature collects and returns extravasated fluids, proteins, dietary lipids and immune cells into the venous circulation. Failure of the lymphatic vessels to develop or function is associated with a severe impairment of fluid homeostasis, tissue integrity and the generation of immune responses (Tammela and Alitalo, 2010; Schulte-Merker *et al*, 2011). Although blood and lymphatic vessels exist and operate in close proximity, it is vital for their function to remain as separate entities. Both systems only connect at the subclavian veins, where the thoracic duct (TD) and right lymphatic duct drain into the venous blood vasculature.

Lymphatic endothelial cells (LECs) differentiate from blood endothelial cells (BECs) in the cardinal vein (CV) after the onset of circulation. In the mouse, differentiation of LECs starts around day 9.0 of embryonic development (E9.0) by polarized expression of the transcription factor Sox18 in dorsolateral cells of the CV (Francois *et al*, 2008), where Sox18 induces expression of the transcription factor Prox1. Prox1 becomes detectable in the CV around E10.0 and Prox1-expressing LECs emerge from the CV and migrate dorsally, where they form the first lymphatic structures (Oliver, 2004).

Prox1-deficient embryos completely lack lymphatic development due to a failure in LECs specification (Wigle *et al*, 2002). Acting as a master regulator of lymphatic development, forced Prox1 expression in cultured BECs confers lymphatic identity (Hong *et al*, 2002; Petrova *et al*, 2002). At present, the signals responsible for the polarized expression of Sox18 and Prox1 in the CV are unknown. Furthermore, directed migration of the emerging LECs depends on the vascular endothelial growth factor C (VEGF-C), which is provided by the lateral mesoderm. Also, *Vegf-c*^{-/-} mouse embryos lack lymphatic vessels and *Vegf-c*^{+/-} mice suffer from lymphatic hypoplasia, demonstrating haplo-insufficiency of a single *Vegf-c* allele for lymphatic development (Karkkainen *et al*, 2004). VEGF-C acts via its tyrosine kinase receptor vascular endothelial growth factor receptor 3 (VEGFR-3) and the non-signalling coreceptor neuropilin 2 (Nrp2) (Karpanen *et al*, 2006; Tammela *et al*, 2010). Extracellular cues for emerging LECs are provided by the matrix-interacting protein collagen and calcium-binding EGF domains 1 (CCBE1), which in a non-cell autonomous fashion strongly augments the pro-lymphangiogenic activity of VEGF-C (Bos *et al*, 2011). In the mouse also CCBE1 is indispensable for lymphatic development because Prox1-expressing *Ccbe1*^{-/-} endothelial cells fail to leave the CV and migrate (Bos *et al*, 2011).

Elegant genetic studies and lineage tracing experiments have confirmed the venous origin of LECs first proposed by Sabin over 100 years ago (Sabin, 1902; Wigle and Oliver, 1999; Srinivasan *et al*, 2007). Yet, despite significant advances

in the identification of genes involved in the formation of the first lymphatic vessels (reviewed in Schulte-Merker *et al*, 2011), the exact morphogenetic mechanisms of initial lymphangiogenesis remain incompletely understood. The initial analysis of *Prox1*-deficient mice suggested budding of newly specified LECs from the CV, followed by dorsal migration and reorganization into large lumenized structures termed as lymph sacs (Oliver, 2004). Unexpectedly, several genes, some of which are exclusively expressed in haematopoietic cells (Abtahian *et al*, 2003; Bohmer *et al*, 2010), have been shown to be important for the separation of blood and lymphatic vessels. These include the lymphatic transmembrane glycoprotein podoplanin (Fu *et al*, 2008; Uhrin *et al*, 2010) and its pro-coagulant receptor on platelets, CLEC-2 (reviewed in D'Amico and Alitalo, 2010). The involvement of platelets in the separation of blood and lymph vessels sparked a new concept, which proposed LECs to emerge from the CV by sprouting. Platelet coagulation at the base of emerging sprouts was hypothesized to trigger the subsequent abscission of newly formed lymphatic vessels from the CV (Kim and Koh, 2010; Uhrin *et al*, 2010). Finally, optical projection tomography reconstructions suggested entire segmental areas of the CV to balloon out and pinch off dorsally. Again aided by platelets, this morphogenetic process would give rise to lymph sacs in a single step (Francois *et al*, 2012). Presently, due to these conflicting models the precise mechanism of the first steps of lymphatic vessel formation remains unclear and requires novel analytical approaches.

In the mouse, progress in understanding lymphatic development has been hampered by limited imaging access. In this study, we have revisited the first steps of lymph vessel formation using ultramicroscopy, a novel technology based on selective plane illumination (Becker *et al*, 2008). We analysed digital 3 dimensional (3D) reconstructions of image stacks obtained by optical sectioning of entire, undistorted embryos. Ultramicroscopy allowed a far more detailed description of initial lymphangiogenesis compared to traditional sections, but also the identification of previously unrecognized structures. Here, we show that lymphatic progenitor cells emerge from the dorsal side of the CV as streams of cells. LECs rapidly accumulate close to the first lateral branch of the intersegmental vessels, where they condensate to form a peripheral longitudinal lymphatic vessel (PLLV), which subsequently gives rise to superficial lymphatics. Simultaneous with PLLV formation, LECs located more closely to the CV aggregate to form a large lumenized structure, which can be considered as the primordial TD (pTD). In *VEGF-C* and *CCBE1*-deficient embryos, *Prox1*-positive LEC progenitors were specified, but displayed distinct migratory defects. While *VEGF-C*-deficient LECs remained stuck inside their venous vessel of origin, loss of *CCBE1* resulted in the formation of aberrant *Prox1*-positive sprouts. Unexpectedly, both mutants provided evidence for a second source of LECs distinct from the CV and located within the lateral venous plexus.

Results

In this study, we aimed to precisely describe the separation of the first LECs from the CV and therefore visualized this process in entire, wholemount-stained mouse embryos. To

overcome the limitations associated with the analysis of consecutive tissue sections, we employed ultramicroscopy, a technology that has become recently commercially available. Ultramicroscopy is a planar illumination microscopy technique, which enabled us to perform optical sectioning of immunostained, cleared, intact mouse embryos at E9.5–E12.0. Illumination with a laminar sheet of light causes the excitation of a thin sample plane, which is recorded orthogonally to the illumination light path by widefield imaging with an area detector, in our case an EM-CCD camera. Ultramicroscopy is particularly suited for the analysis of developmental processes in large specimen. Because axial and lateral resolution scale with the inverse numerical aperture of the illumination and detection optics ($1/NA_{\text{ill}}$ and $1/NA_{\text{det}}$) both parameters can be adjusted to obtain an isotropic point spread function when using this technology (Supplementary Figure 1). Despite the use of low magnification and low numerical aperture optics, image stacks covering entire wholemount immunostained mouse embryos with comparable lateral and axial resolution reaching the level of individual cells were obtained (Figure 1A–D).

The first lymphatic endothelial progenitors emerge as streams of cells from the roof of the CV

To identify landmark structures of the developing vascular system, we performed wholemount immunostaining for PECAM-1, which was expressed on all vessels, however, with varying intensity. Invariably, arterial vessels displayed the strongest PECAM-1 expression followed by veins, while the lymphatic vessels showed weakest expression. Therefore, strong PECAM-1 staining depicted the arterial vasculature in 3D reconstructions, readily identifying prominent structures like the dorsal aorta (DA), intersegmental arteries (ISA), the pharyngeal arch arteries (PAA) and the developing heart (Figure 1A and B). In contrast, *VEGFR-3* and the sialomucin Endomucin predominantly stained venous vessels and were therefore suitable as surrogate venous markers (Figure 1C and D). Endomucin expression was particularly pronounced on small venous vessels and we found its expression maintained throughout development while *VEGFR-3* expression was, as described (Kaipainen *et al*, 1995), downregulated on venous vessels parallel to the formation of the first lymphatics (see also Supplementary Figure 2; Figure 6I).

Between E9.5 and E12.0 of mouse development, the CV is a paired, fully symmetrical structure (Figure 1F). Anterior and posterior CVs are connected via the common cardinal vein (CCV) from which the sinus venosus (SV) drains venous blood ventrally to the developing heart (Figure 1E and blue arrows in F).

We detected the first *Prox1*-expressing (*Prox1*⁺) ECs at E10.0 in the CCV, dorsally opposite the SV (Figure 1H, J, L and M). Simultaneously with the appearance of *Prox1*⁺ cells in the CV, LECs emerged from the dorsal roof of the CV (Figure 1H–M). *Prox1*⁺ cells leaving the CV appeared as streams of spindle shaped cells (Figure 1J, K, N and O). Because the dorsally emerging *Prox1*⁺ LECs were the first discernible LECs outside the CV, we refer to them as initial LECs (iLECs).

Within the meshwork formed by iLECs, cells were frequently connected by very thin processes (Figure 2A, white arrowheads). We regularly found erythrocytes, which were easily discerned by their shape and autofluorescence, enclosed within arterial and venous vessels of various calibre

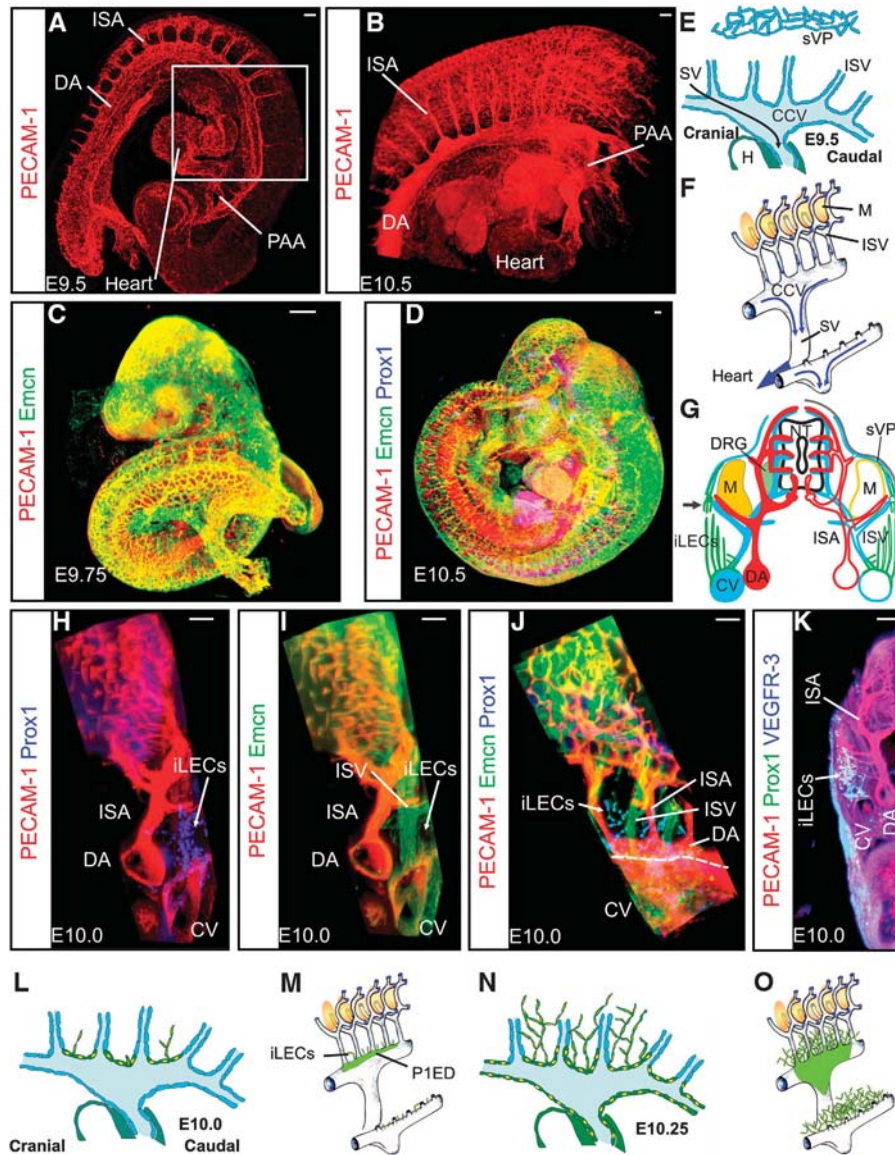


Figure 1 Emergence of the initial lymphatic progenitor cells from the cardinal vein. (A–D) Wholemount immunostaining of the vasculature in mouse embryos at 9.5/9.75 (A, C) and 10.5 (B, D) days post fertilization. PECAM-1 preferentially stained arterial, Endomucin mostly venous vessels. Prox1 identified lymphatic endothelial cells (LECs). The box in (A) delineates the jugular-thoracic region, in which LECs emerged from the cardinal vein (CV). DA, dorsal aorta; ISA, intersegmental artery; PAAs, pharyngeal arch arteries. Scale bar = 100 μm. (E) Schematic sagittal section through one of the paired CVs. Venous ECs, blue; developing heart, dark green. The relative position of the superficial venous plexus (sVP) is indicated. CCV, common cardinal vein; SV, sinus venosus; H, heart; ISV, intersegmental vein. (F) 3D representation of the paired CCVs and SV draining into the heart. Depicted on the averted half of the symmetrical CVs are the ISVs and myotomes (M). Blue arrows indicate the flow of venous blood. (G) Schematic transverse section at the jugular-thoracic region. DA, ISA and arterial plexus in red; CV, ISV and sVP in blue. NT, neural tube; DRG, dorsal root ganglion; iLECs, initial lymphatic endothelial cells. (H–K) Volume reconstruction of optical sections of embryos wholemount immunostained for the proteins noted on the left side of each panel. E, developmental stages in days post fertilization. (H, I, K transverse sections; J sagittal sections). White arrows, emerging iLECs; dotted line, dorsal roof of the CV. Scale bar = 100 μm. (L–O) Schematic depiction of the emergence of the first iLECs between E10.0 and E10.25. Prox1+ cells, green with yellow nuclei. The Prox1 expression domain (P1ED) in the averted branch of the CCV is indicated as a green surface.

(Figure 2A, red arrowheads), however, we never detected erythrocytes enclosed by migrating iLECs. Staining for the endothelial junction protein VE-cadherin suggested that iLECs were not enclosing a lumen (Supplementary Figure 5G).

Upon egress from the CV, emerging iLECs underwent a pronounced change in cell shape from squamous to spindle shape (Figure 2B compare Prox1+ cells in the CV (arrow) and iLECs). This cellular shape change was accompanied by a change in nuclear shape from round to oblong (Figure 2D

and E). In addition, the transition was associated with an upregulation of Prox1, VEGFR-3 and its coreceptor Nrp2 in iLECs (Figure 2C and F–H).

Concomitantly with the massive appearance of iLECs outside the CV, VEGFR-3 expression was lost from venous vessels (Figure 2B) and was hardly detectable after E11.0. In contrast, Endomucin expression was maintained on venous endothelium, but rapidly lost from iLECs and no longer detectable on LECs after E12.0 (see also Figure 6C and I).

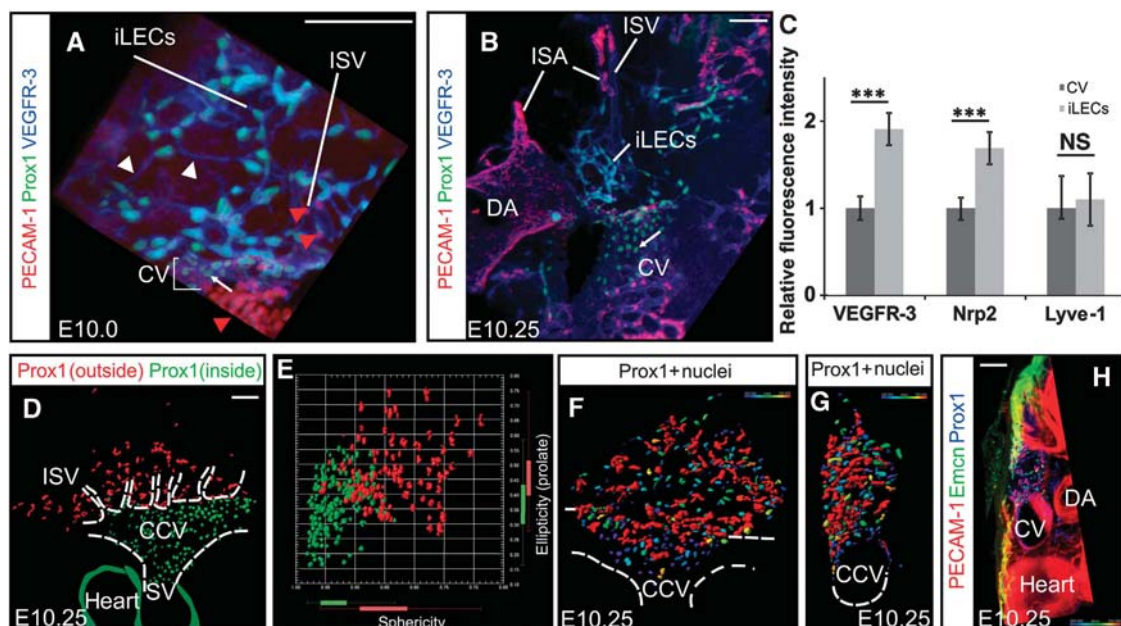


Figure 2 Budding of lymphatic endothelial cells from the CV is associated with a change in cell and nuclear shape, but also with a switch in protein marker expression. (A, B) Sagittal view of the CCV of embryos wholemount immunostained for the proteins indicated on the left side of each panel. Developmental stages in days post fertilization (E); iLECs, initial lymphatic endothelial cells; cranial, left; caudal, right. Scale bar = 100 μ m. Upon egress from the CV, LEC shape changed from squamous (arrows indicate Prox1 + ECs in the roof of the CV) to spindle shape. White arrowheads, extremely thin connections between iLECs; red arrowheads, erythrocytes frequently found in lumenized venous vessels (but never in iLECs). (B) Also see corresponding scheme Figure 10. (C) At E10.5, VEGFR-3 and its co-receptor Nrp2 were upregulated in emerging iLECs, while Lyve-1 levels remained unchanged in the CV and iLECs. *** $P \leq 0.001$, NS, non-significant. (D, E) Nuclear shape change from spherical to elliptical associated with the emergence of iLECs. Nuclei of Prox1 + cells outside (red) and within (green) the CCV were depicted by nuclear surface rendering (D) and plotted against sphericity and ellipticity (prolate) (E). Scale bar = 100 μ m. (F–H) Surface rendering of Prox1 + nuclei inside and outside the CCV of wholemount immunostained embryo in sagittal (F) and transversal view (G, H). (F, G) Prox1 expression strength is indicated by pseudo-colouring using a heat map, i.e. highest Prox1 expression is indicated in red, low expression in blue. (H) Anatomical location of cells is depicted by superposition. Software package: Imaris Vantage, Scale bar = 100 μ m.

Between the developmental stages E10.0 and E10.25, the number of strongly Prox1+ iLECs dorsally of the CV increased dramatically, resulting in a massive density augmentation of the iLEC meshwork (Figures 1H, K and 2A). During this process, integrity of the CV was not impaired and we did not detect a deformation of or protrusions from the dorsal roof of the CV (Figures 1J and 2A). At the same time, the Prox1 expression domain rapidly expanded over the CCV into the sinus venosus and Prox1 expression was also initiated in the developing heart (Figures 1N, O and 2D).

Initial LECs condensate to form a PLLV laterally underneath the myotome

During development, a major branch of the ISAs and inter-segmental veins (ISVs) extends laterally towards the body surface. This side branch is located laterally underneath the myotomes and connects to the superficial capillary plexus (black arrow in schematic transverse section in Figure 1G). The majority of iLECs were detected between the CV and ventral to these major ISA and ISV side branches (Figures 1H, K, 3A and C), although already at E10.5 iLECs were also detected more dorsally (Figure 3B).

While we reproducibly detected the first Prox1 + cells at E10.0 in the dorsal roof of the CV, we cannot exclude that during the subsequent rapid increase iLECs emerged from other venous vascular beds, in particular the ventral edge of the superficial venous plexus (sVP) (Figure 1E and G). We have indicated the relative position of this venous plexus in Figure 3G and H.

Between the CCV and the ISA/ISV side branches, iLECs spread cranially and caudally, resulting in a fan-shaped distribution (Figure 3A). Around E10.5, we observed a rapid accumulation of LECs at the dorsal edge of the iLEC meshwork. The iLEC condensation resulted in the formation of lumenized structures, which upon coalescence formed a longitudinal vessel in this peripheral position, which we denoted as PLLV. The corresponding stripe is indicated as PLLV condensation zone in Figure 3A–D. In contrast to the DA and CV, the PLLV was rather irregularly shaped along the longitudinal embryonic axis (note the multiple intersections with small, lumenized LEC aggregates in the PLLV condensation zone in Figure 3D). Due to its convoluted shape (Figure 3B–D), the PLLV is therefore easily missed in thin optical (Figure 3D) or histological sections.

Simultaneously with the formation of the PLLV, we observed the appearance of longer, contiguous lymphatic structures that extended dorsally from the PLLV. We presume that these LECs subsequently formed the dorsal superficial lymphatic plexus and refer to them therefore as superficial LECs (sLECs) (Figure 4B–D). In accord with a migratory or active sprouting behaviour, sLECs displayed high VEGFR-3 and Nrp2 expression, but in contrast to iLECs showed strongly reduced Lyve-1 levels (Figure 4I).

The pTD is formed by aggregation of initial LECs close to the CV

Simultaneously to the condensation of iLECs resulting in formation of the PLLV, we noted the aggregation of iLECs

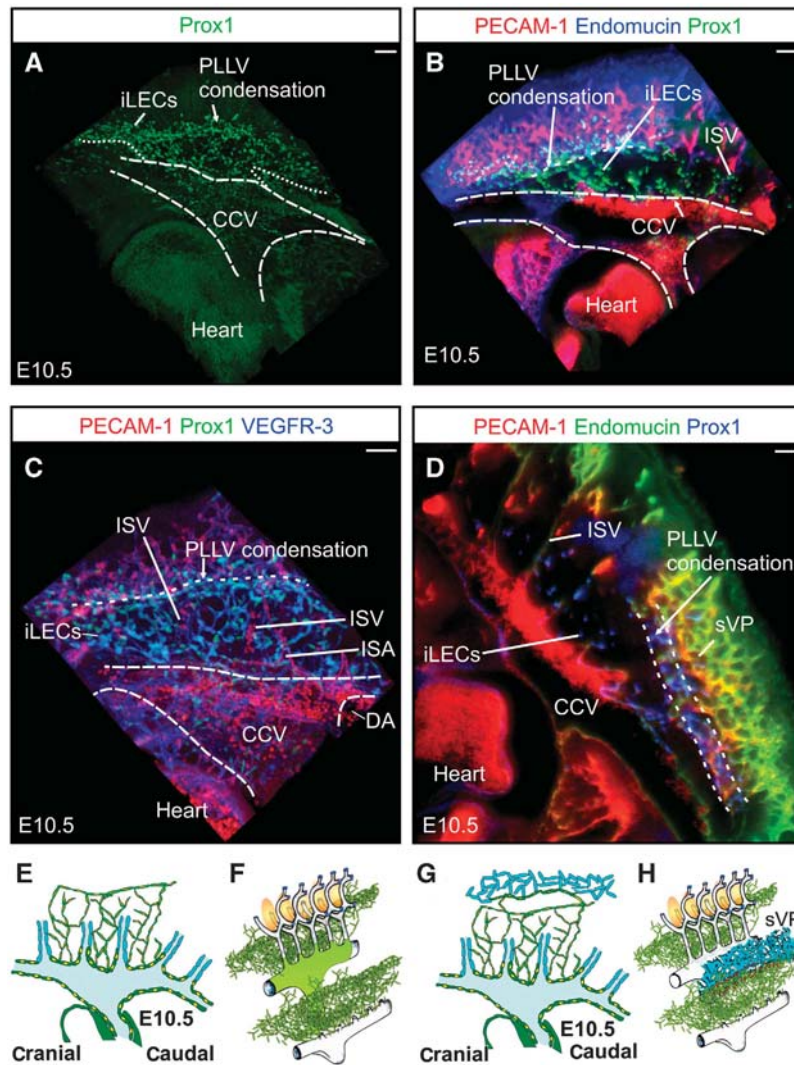


Figure 3 iLECs condense at the level of the major lateral branch of the intersegmental vessels to form a lumenized peripheral longitudinal lymphatic vessel (PLLV). (A–D) Sagittal view reconstructed from optical sections of embryos wholemount immunostained for the proteins indicated above each panel. E, developmental stages in days post fertilization; cranial, left; caudal, right. (A) During the first stages of iLECs emergence, iLECs appeared in a fan-shaped pattern, which extended caudally and cranially from the CCV. Dotted line, ventral border of iLEC detection. (A–D) iLECs immediately condensed at the level of the first lateral branch of the intersegmental vessels to form the PLLV. Long-hatched lines denote the position of the CCV and SV; short-hatched line, area of iLECs condensation and PLLV formation. (E–H) Schematic depiction of the position of iLECs appearing dorsal to the CV between E10.5 and E10.75. Prox1 + iLECs outside the CCV are depicted in light green, Prox1 + cells within the CV and heart muscle in dark green. The Prox1 expression domain (P1ED) in the averted branch of the CCV is indicated as a light green surface. Position of the superficial venous plexus, as a possible alternative source of iLECs, is indicated in blue (G, H). Prox1 + endothelial cells within the sVP are highlighted in red. sVP, superficial venous plexus; scale bars = 100 μ m.

more closely located to the CV (Figure 4A, white arrowheads). Between E10.5 and E11.0, this process proceeded rapidly and resulted in the appearance of agglomerates or nests of iLECs, which also lumenized and gave rise to a larger structure. This newly formed lymphatic vessel was clearly separate from the PLLV and it developed in close proximity to the CV, to which it actually had physical contact (Figure 4B and E–H). Towards its cranial end, it was connected via a bow-shaped structure with the PLLV (Figure 4B, C and E–H).

These unique properties were highly reminiscent of the TD, which at completion of fetal development, constitutes the largest lymphatic vessel. The pTD develops anatomically in a position corresponding to the location of the mature TD. Therefore, we suggest referring to the largest, lumenized,

embryonic lymphatic structure with direct physical contact to the CV as pTD (Figure 4B–D). At developmental stage E11.5, the pTD was fully developed and while dorsally sprouting sLECs originated from the PLLV, more laterally directed sprouts emanated preferentially from the pTD (Figure 4C and D). We would like to emphasize that at midgestation and during early fetal development both PLLV and pTD constitute bilateral, fully symmetrical structures.

High levels of Prox1 expression at the contact site of pTD and CV

We were particularly intrigued by the tandem contact sites that stereotypically formed between each pTD and the CCV. Starting at E11.5, these contact points were readily identified

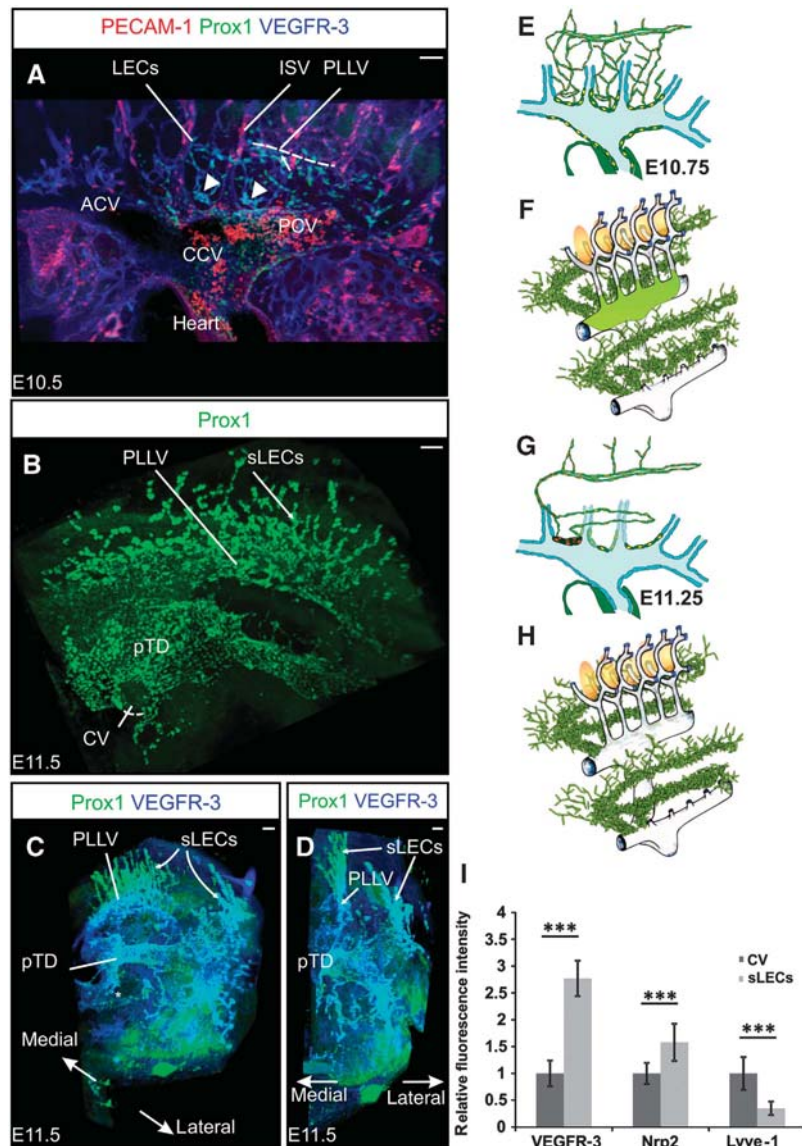


Figure 4 LECs between the CV and PLLV aggregate and form increasingly larger lumenized structures finally giving rise to the primordial thoracic duct. (A–C) Sagittal and (D) transversal views reconstructed from optical section of embryos wholemount immunostained for the proteins indicated above each panel. (A) Arrowheads indicate rapid and progressive aggregation of LECs located between CV and PLLV, which resulted in the formation of a large lumenized structure, the pTD (B–D). (C, D) Superficial lymphatics (sLECs) appeared to sprout from the PLLV dorsally and the pTD laterally. PLLV and pTD were connected at the cranial end of the pTD. (F–H) Schematic depiction of the cellular aggregation/condensation events that result in pTD formation. (I) At E11.5, VEGFR-3 and its co-receptor Nrp2 were upregulated in sLECs, while Lyve-1 levels were strongly reduced as compared to the CV and iLECs. $***P \leq 0.001$. Developmental stages in days post fertilization (E); cranial, left; caudal, right. ACV, anterior cardinal vein; CCV, common cardinal vein; PCV, posterior cardinal vein; ISV, intersegmental vein; PLLV, peripheral longitudinal lymphatic vessel; pTD, primordial thoracic duct; sLECs, superficial lymphatics. Scale bars = 100 μ m.

by their exceptionally high Prox1 expression (Figure 5A and B, white arrowheads). While we had noted that Prox1 was upregulated in migrating iLECs after egress from the CV, Prox1 expression decreased again upon aggregation and incorporation of iLECs into the pTD, albeit the pTD clearly remained Prox1+. In contrast, sLECs of the developing dorsal and lateral superficial lymphatics retained high Prox1 expression, however as previously described (Norrmen *et al*, 2009), completely lost Lyve-1 expression. By far the strongest Prox1 expression was detectable in the LECs at the contact site between pTD and CV (Figure 5A–E, white arrowheads). At E12.0, Prox1 was no longer expressed in the CCV or SV, with exception of the ECs directly opposing

the pTD (Figure 5E, arrows). Both, the ECs of the CCV and the pTD, strongly expressed Prox1, hence, the immediate contact site was formed by a double layer of highly Prox1+ ECs (Figure 5E). Intriguingly, the tandem contact sites between pTD and CCV always flanked an arterial vessel, which transverse the CV (Figure 5B–E, white asterisk). This arterial vessel, which we identified as a side branch of the developing subclavian artery (Supplementary Figure 3; Supplementary Video 1), was in direct contact with the CV (Figure 5E).

Starting at day E12.0, we often detected densely packed erythrocytes within the lumen of the pTD adjacent to the CV (Figure 5C, red arrowhead), suggesting the development of a direct connection between both structures. Based on this

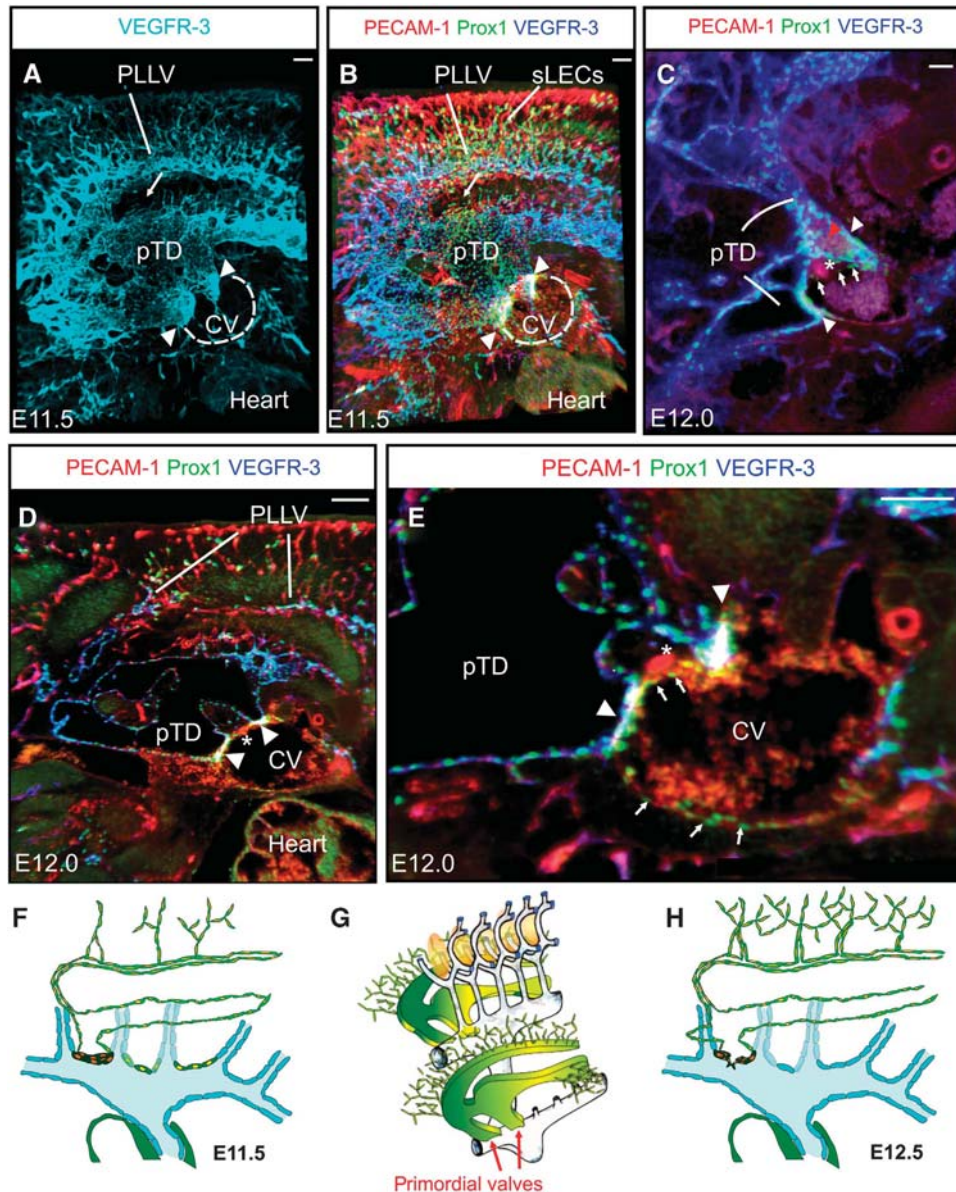


Figure 5 Paired contact sites between the newly formed pTD and the CV are characterized by highest levels of Prox1 expression. (A–C) Sagittal views of wholemount immunostained embryos. The newly forming pTD rapidly consolidated into a massive lumenized structure, cranially connected in a U-shape to the PLLV (left side A, B). Two contact sites between CV and pTD expressed high levels of Prox1 (arrowheads). (B–E) An arterial vessel identified as a transient side branch of the subclavian artery and stereotypically located between the contacts of pTD and CV is marked by an asterisk. (C) Red arrowhead: packed erythrocytes within the pTD. Arrows denote Prox1+ cells in the CV opposing the pTD contact sites. (D, E) Individual planes (optical sections) through the contact area of pTD and CV. (F–H) Schematic representation of the development of the contact sites between pTD and CV with highly Prox1+ cells at the contact site depicted in dark green with red nuclei. Scale bars = 100 μ m.

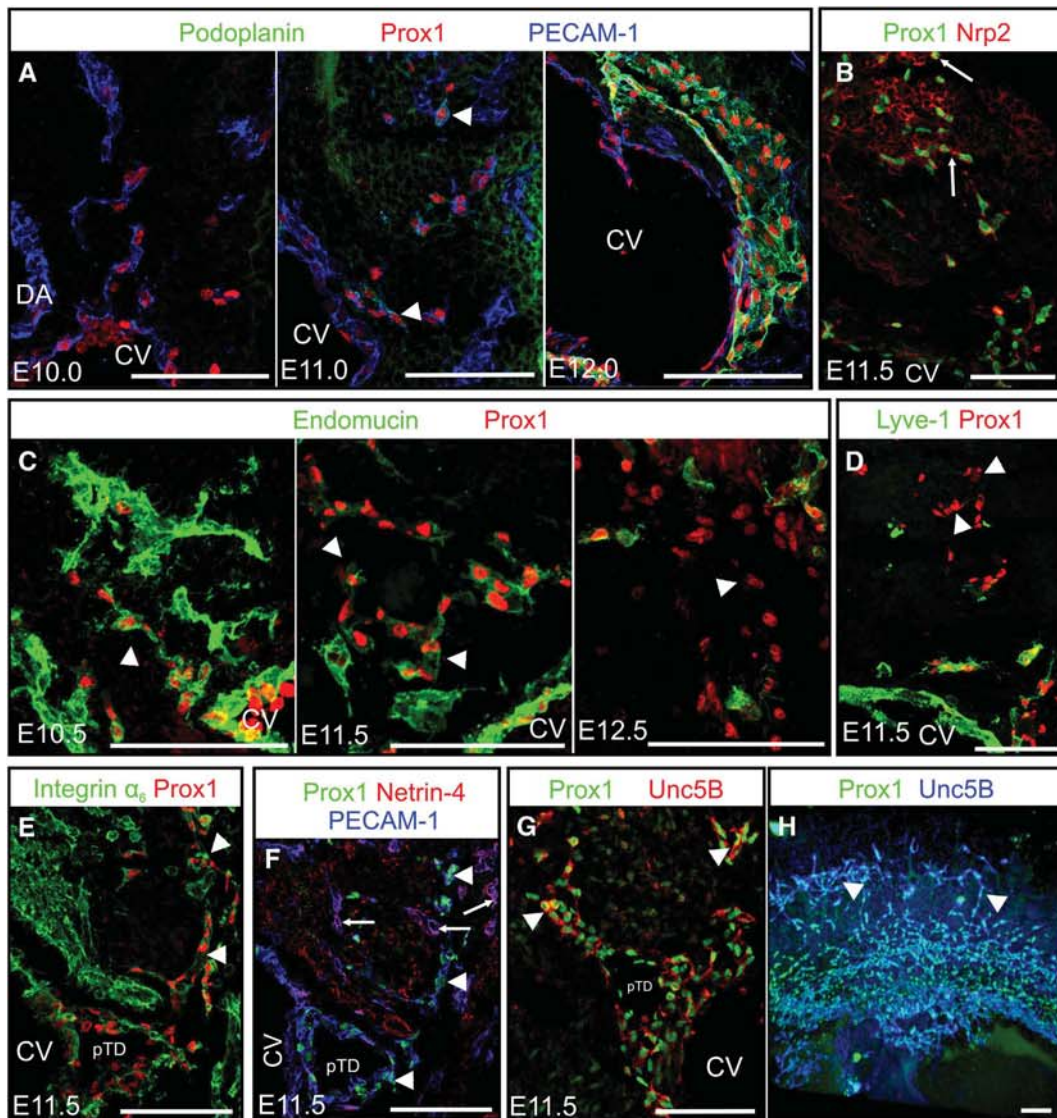
frequently recurring observation and the high expression of Prox1, we speculate that the contact sides between pTD and CV might develop into first valves, allowing the developing lymphatics to become functional by preventing backflow from the venous circulation into the nascent lymphatic vasculature.

Distinct gene expression patterns characterize different LEC populations

To obtain further insight into the molecular mechanisms regulating the first steps of lymph vessel development, but also to validate our wholemount analysis, we stained for the

expression of cell surface markers or secreted proteins known to be important for vascular development. Suitable antibodies for wholemount staining were only available for some proteins, therefore, we evaluated immunostaining of cryosections in parallel (results are summarized in Figure 6I). As expected, in most sections it was not possible to identify the PLLV unambiguously. Therefore, we distinguished Prox1+ ECs within the CV from emerging iLECs and LECs within the lumenized pTD from sLECs of the forming superficial lymphatics.

The transmembrane glycoprotein podoplanin (Pdpn) is expressed within the vascular system in a lymphatic-specific manner (Schacht *et al*, 2003) and has been identified as a



I

Gene	Struct.	E10.0	E10.5	E11.0	E11.5	E12.0	E12.5
Prox1	CV						
	iLECs						
	sLECs						
	pTD						
PECAM-1	CV						
	iLECs						
	sLECs						
	pTD						
VEGFR-3	CV						
	iLECs						
	sLECs						
	pTD						
Emcn	CV						
	iLECs						
	sLECs						
	pTD						
Podpn	CV						
	iLECs						
	sLECs						
	pTD						
Lyve-1	CV*						
	iLECs						
	sLECs						
	pTD						
Nrp2	CV*						
	iLECs						
	sLECs						
	pTD						
Unc5B	CV*						
	iLECs						
	sLECs						
	pTD						
Netrin-4	CV						
	iLECs						
	sLECs						
	pTD						
Integrin α ₆	CV						
	iLECs						
	sLECs						
	pTD						
VEGFR-2	CV						
	iLECs						
	sLECs						
	pTD						
Integrin β1	CV						
	iLECs						
	sLECs						
	pTD						

Gene	Struct.	E10.0	E10.5	E11.0	E11.5	E12.0	E12.5
Nrp2	CV*						
	iLECs						
	sLECs						
	pTD						
Unc5B	CV*						
	iLECs						
	sLECs						
	pTD						
Netrin-4	CV						
	iLECs						
	sLECs						
	pTD						
Integrin α ₆	CV						
	iLECs						
	sLECs						
	pTD						
VEGFR-2	CV						
	iLECs						
	sLECs						
	pTD						
Integrin β1	CV						
	iLECs						
	sLECs						
	pTD						

	Strong expression		Expressed on dorsal site of CV
	Moderate expression		* On dorsal site of CV
	Low expression		Not determined
	Not expressed		Structure not yet developed

surface-bound ligand for the platelet C-type lectin CLEC-2 (Suzuki-Inoue *et al*, 2007). Pdpn-mediated CLEC-2 activation is pro-coagulant and essential during the separation of blood and lymphatic vessels (Uhrin *et al*, 2010). In agreement with a recent study (Francois *et al*, 2012), we detected no Pdpn expression on Prox1+ cells in the CV. Moderate Pdpn expression started at E11.0 on the nascent pTD and sLECs, while iLECs remained negative (Figure 6A–I; Supplementary Figure 4). By E11.5, Pdpn was strongly expressed on all lumenized and peripheral lymphatic structures.

A second common marker of adult peripheral lymphatics, in particular lymphatic capillaries, is the hyaluronan receptor LYVE-1. As described (Norrmen *et al*, 2009; Tammela *et al*, 2010), we found strong, polar expression of Lyve-1 on Prox1+ cells in the dorsal half of the CV, which was maintained on the emerging iLECs and nascent lumenized structures (pTD) (Figure 6D and I; Supplementary Figure 4A, B, D and E). Lyve-1 was not or only weakly detectable on sLECs (Figure 4I), however, it was again found re-expressed on skin lymphatics at E14.5 (not shown).

Netrins, laminin-related, secreted axon guidance molecules and their Unc receptors are involved in patterning during vessel growth (Adams and Eichmann, 2010). Hence, we were particularly interested to analyse the expression of Netrin-4, a pro-lymphangiogenic factor (Larrieu-Lahargue *et al*, 2010), on emerging lymphatics. Netrin-4 was expressed on blood vessels, but not on iLECs or sLECs. Lymphatic Netrin-4 expression started around E11.5 on the pTD (Figure 6F; Supplementary Figure 6E–H). In contrast, the canonical netrin receptor Unc5B was expressed on the pTD and sLECs starting at E11.0 (Figure 6G and H; Supplementary Figure 7). The pro-lymphangiogenic activity of Netrin-4 appears to be mediated by integrins, in particular integrin $\alpha 6 \beta 1$, rather than Unc receptors (Larrieu-Lahargue *et al*, 2011). We therefore tested the presence of $\alpha 6$ integrins on LECs and found it homogeneously expressed on lumenized structures and sLECs from E11.0 onwards (Figure 6E; Supplementary Figure 6A–D) while integrin $\beta 1$ was present on all Prox1+ LECs at E10.5 and E11.5 (Supplementary Figure 6M–P). Surprisingly, we did not detect integrin $\alpha 9$ expression on Prox1+ LECs at E10.5 and E11.5, while using the same reagents and protocol $\alpha 9$ was clearly present on the pTD at E13.0 on developing lymphovenous valves (Supplementary Figure 6Q–T).

VEGFR-3 is necessary for proper pTD formation and sLEC patterning

While the receptor tyrosine kinase VEGFR-3 is indispensable for blood vascular development, it is also a key regulator for

lymphangiogenesis (Tammela *et al*, 2008). Mice deficient for VEGFR-3 die at E10.5 at the onset of lymphangiogenesis due to cardiovascular defects (Dumont *et al*, 1998). Therefore and in the absence of an inducible VEGFR-3 knockout, our analysis was limited to heterozygous embryos. In *Vegfr3*^{+/-} embryos the main lymphatic structures PLLV, pTD and sLECs formed (Supplementary Figure 9F). Also formation of the contact sites between CV and pTD appeared unimpaired (Supplementary Figure 9F, G and I). However, consistent with monoallelic VEGFR-3 expression, iLEC numbers outside the CV were reduced (Supplementary Figure 9F) and the sLECs meshwork was mispatterned. Y-shaped sLEC structures, which were frequently detected in wild-type littermates, were absent in *Vegfr3*^{+/-} embryos (Supplementary Figure 9B and G). Most prominently, the pTD appeared disrupted and of smaller diameter (Supplementary Figure 9D and I).

CCBE1 deficiency results in a failure of nascent LECs to leave the veins, formation of aberrant venous sprouts and a lack of developing lymphatic vessels

CCBE1 is an extracellular matrix component essential for lymphatic vessel development. Genetic ablation of CCBE1 results in the loss of definitive lymphatic structures in the mouse and zebrafish (Bos *et al*, 2011). From LacZ-wholemount stainings of mouse embryos, we concluded that CCBE1 is expressed in areas associated with lymphatic development from E10.5 onwards (Supplementary Figure 10). At day E10.5, Prox1+ ECs developed in the CV of *Ccbe1*^{-/-} embryos (Figure 7B, D and F). The expression domain of Prox1 appeared to extend into the ISVs and Prox1+ cells accumulated in the CV. More unexpected, we also found Prox1+/VEGFR-3+ cells in a rudimentary form of the PLLV, while the iLEC meshwork between CV and PLLV was completely absent (Figure 7B, D and F). Prox1+ LECs, which aligned at the PLLV condensation zone, were part of aberrant sprouts that originated from the intersegmental vessels, but also from the ventral edge of the sVP (Supplementary Figure 11C and D). Also from the CV, Prox1+/VEGFR-3+ cells formed dilated sprouts or bag-like sacs, which always remained connected with the CV (Figure 7B, D and F; Supplementary Figure 11A–D; Supplementary Video 2). While at E10.5 the observed dysmorphic sprouts were highly Prox1+, 1 day later at E11.5, Prox1 expression was undetectable in *Ccbe1*^{-/-} embryos (Figure 7F and G; Supplementary Figure 11E). The PLLV rudiment was no longer detectable, however, there were still sprouts projecting from the ISVs (Figure 7F and G). Prox1 expression was also

Figure 6 Different lymphatic endothelial cell populations express distinct sets of marker proteins. (A–G) Immunostainings of transversal cryosections from embryos at the indicated developmental ages are shown. Visualized antigens are depicted in the corresponding colours indicated above each panel. Panels exemplify representatively the marker expression summarized in (I). (A) Podoplanin expression was absent on LECs at E10.0, was first detectable at E11.0 (arrowheads) and was abundant on LECs at E12.0. Note Prox1+ cells in the CV were negative at all stages. (B) At E11.5, Nrp2 was moderately expressed on the CV and the pTD, while iLECs emerging outside the CV were strongly positive (arrows). (C) Endomucin was only transiently retained on iLECs. (D) Lyve-1 was strongly expressed on Prox1+ ECs of the CV and the pTD, while sLECs showed only residual expression (arrowheads). (E) Integrin $\alpha 6$ was moderately expressed on all vascular structures. (F) At E11.5, Netrin-4 was expressed strongly on BECs (arrows), weakly on the CV and moderately on the pTD, but was undetectable on iLECs (arrowheads). (G, H) Unc5B was strongly expressed on iLECs (G, arrowheads) and sLECs (H, arrowheads), while it was weak on the pTD. (H) Sagittal projection reconstructed from optical sections of a wholemount immunostained embryo for Prox1 (green) and Unc5B (blue). (I) Expression of the indicated proteins in different LEC populations during midgestation. Data are based on either immunostained cryosections or wholemount immunostaining. Indicated structures and cell populations: CV, cardinal vein; iLECs, initial LECs (first wave of LECs emerging from the CV as spindle shaped, loosely connected cells); sLECs, superficial LECs (LECs extending from the PLLV (dorsally)); pTD, primordial thoracic duct. CV*, expression limited to Prox1+ cells on the dorsal side of the CV. Scale bars = 100 μ m.

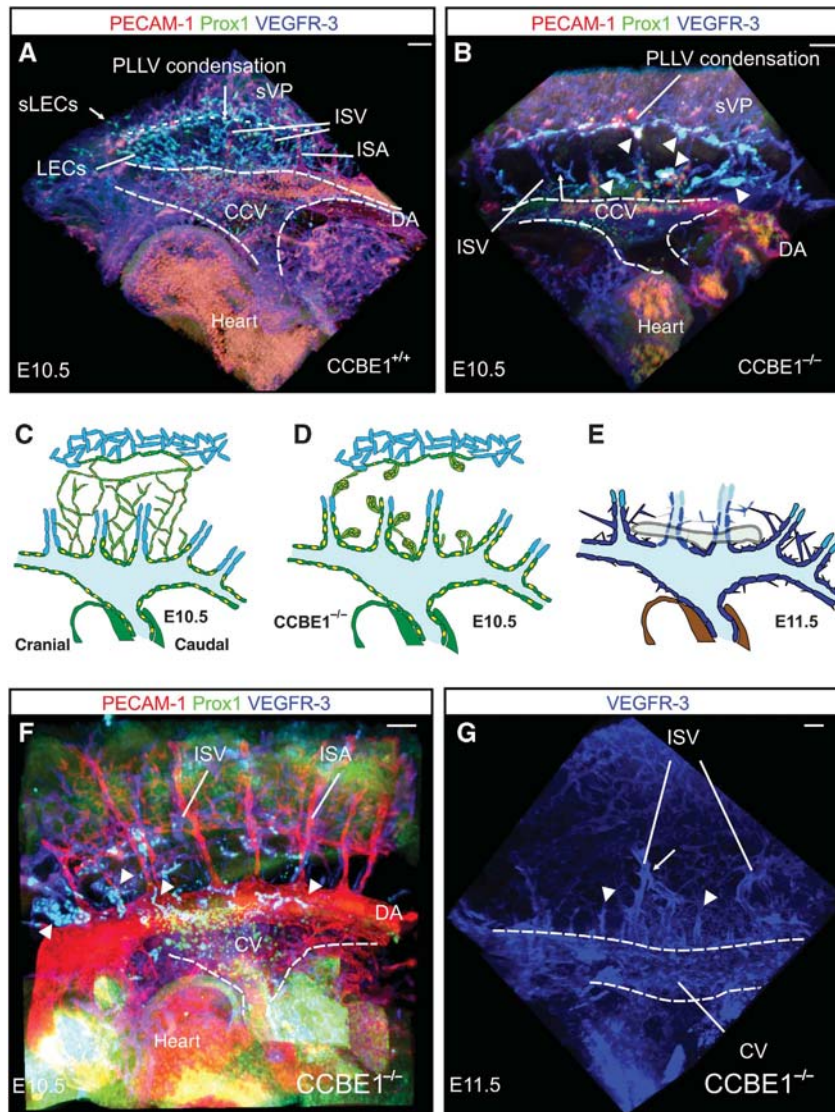


Figure 7 CCBE1 deficiency results in a failure of Prox1⁺ cells to separate from the CV and in rapid loss of nascent lymphatic structures. (A, B, F, G) 3D reconstructions of wild-type (A) and *Ccbe1*^{-/-} (B, F, G) embryos, wholemount immunostained for the indicated proteins. (A, B) Sagittal view at E10.5. (B) In CCBE1-deficient embryos, abundant Prox1⁺ cells were detected in the CV and in a rudimentary PLLV, adjacent to the superficial venous plexus. In contrast to wild-type embryos (A), the meshwork of spindle shaped iLECs between CCV and PLLV was absent. (B, F) Prox1⁺ cells outline the CCV and SV, while atypical, large, lumenized sprouts emerged from the CV (arrowheads). (G) Highly VEGFR-3⁺, dysformed sprouts extended from the CV (arrowheads) and ISVs (arrow). (C–E) Schematic representation of Prox1⁺ cells in wild-type (C) and CCBE1-deficient (D, E) embryos. Strongly VEGFR-3⁺ venous endothelium is depicted in dark blue. sVP, superficial venous plexus; scale bars = 100 μ m.

lost from the CV and the underlying developing heart. Notably, VEGFR-3 appeared strongly upregulated in venous vessels (Figure 7E and G) and in the malformed sprouts, which protruded from the ISVs over the entire length of the CCV (Supplementary Figure 11E). We detected several instances where irregular longitudinal sprouts appeared to form connections between the ISVs.

In VEGF-C-deficient mice, LECs remain trapped in the venous vasculature, revealing their origin

VEGF-C has been shown to be indispensable for the mobilization of LEC progenitors from their venous origin (Karkkainen *et al*, 2004). For instance, in *Vegfc*^{-/-} mice Prox1⁺ LECs fail to migrate from the CV. When we analysed VEGF-C-deficient embryos by ultramicroscopy, we detected at

E10.75 a rich accumulation of Prox1⁺ LECs in the CCV, while there were no iLECs detected outside the CV (Figure 8D–F). Like previously observed in *Ccbe1*^{-/-} embryos, VEGFR-3 expression in the ISVs and sVP was elevated (Figure 8C and E). Remarkably in *Vegfc*^{-/-} embryos, we detected a venous vessel at the ventral edge of the sVP, which massively contained Prox1⁺ cells (Figure 8E and F, white arrowhead), strongly supporting our previous suspicion that also the ventral edge of the sVP is a source of LEC progenitors (Supplementary Video 3).

CCBE1 and VEGF-C interact synergistically during directed migration of iLECs

In addition to its function in lymphatic development, CCBE1 has been described to increase the pro-lymphangiogenic

activity of VEGF-C in the mouse (Bos *et al*, 2011). Therefore, we decided to analyse developing mouse embryos of *Ccbe1* and *Vegfc* compound heterozygotes. Wholemount immunostainings of *Vegfc*^{+/-} at E10.5 revealed a reduced number of Prox1+ iLECs outside the CV (Figure 9D–F), while *Ccbe1*^{+/-} embryos in addition showed an irregular formation of ISVs and Prox1-positive, lumenized sprouts extending from the dorsal roof of the CV (Figure 9G–I). In spite of this early phenotype, CCBE1 heterozygous mice developed normally and showed no lymphatic phenotype at later developmental stages (not shown). In double heterozygous littermates, the reduction of iLECs, but also the formation of aberrant sprouts and abnormal ISV formation were exacerbated, indicating a synergistic interaction of both pathways (Figure 9J–L).

Discussion

Significant progress in the understanding of the molecular control of lymphangiogenesis has to date implicated >20 genes in the control of lymphatic vessel growth and behaviour (Tammela *et al*, 2010; Schulte-Merker *et al*, 2011). Lineage tracing experiments using genetically modified mice provided direct evidence for a venous origin of the lymphatic endothelium (Srinivasan *et al*, 2007), yet a precise description of the morphogenetic events during the separation of the emerging lymphatic from venous endothelium is still missing. To obtain a precise understanding of this process, we applied optical sectioning of cleared wholemount immunostained mouse midgestation embryos, using the planar illumination technique ultramicroscopy (Becker *et al*, 2008). Volume reconstruction of the obtained image stacks allowed a comprehensive analysis, which provided by far more detail than immunostained serial sections.

Based on the existing literature, we started our analysis with E9.5 mouse embryos and first detected polarized Prox1 expression in ECs of the dorsal roof of the CCV at E10.0. Between E10.0 and E10.5, we observed a rapid expansion of the Prox1 expression domain over the entire CCV, also extending into the SV. Simultaneously, Prox1 expression was initiated in the developing heart and finally also detected at the ventral edge of the sVP.

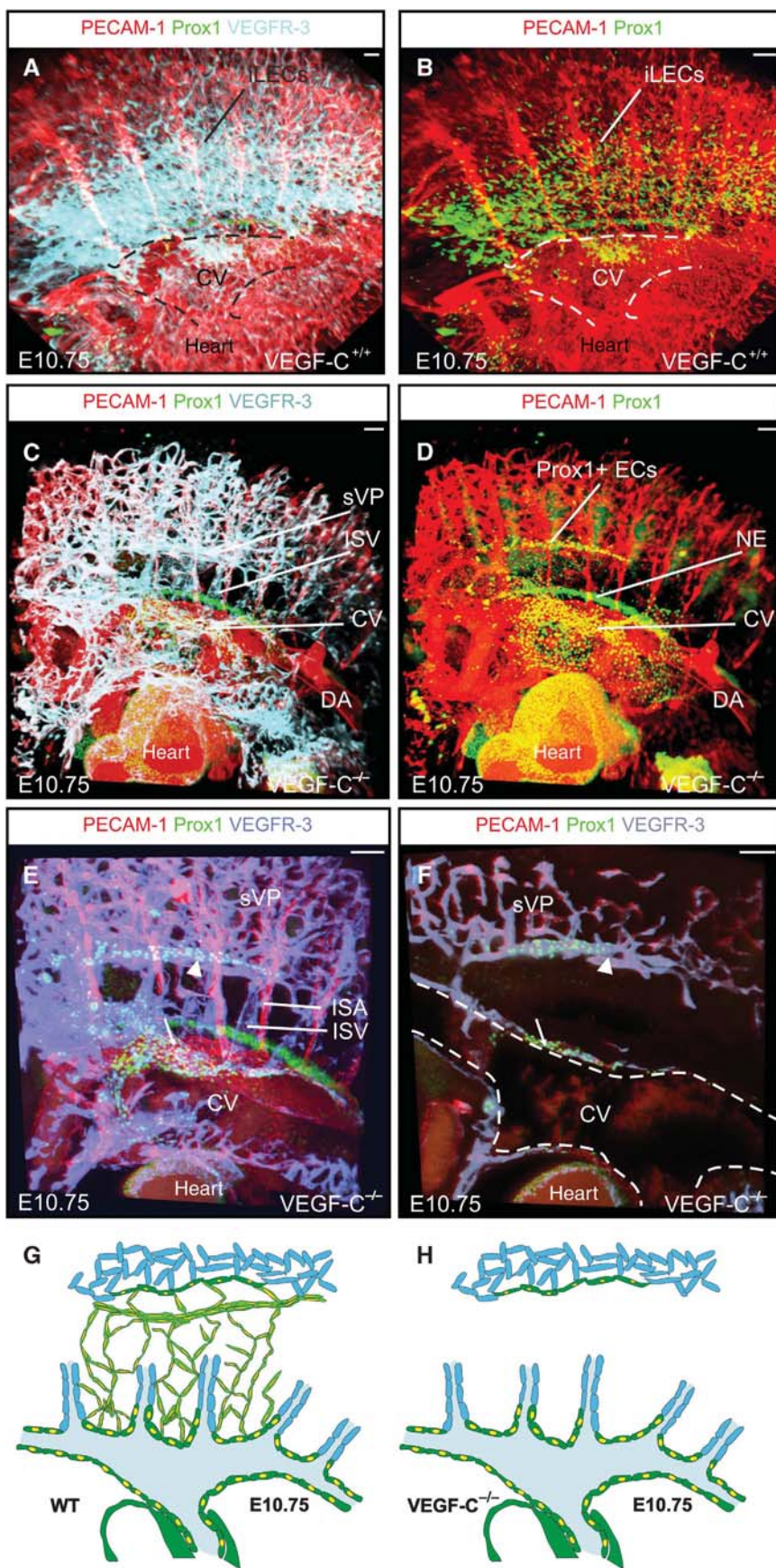
The onset of Prox1 expression in the CCV coincided with the emergence of the first Prox1+ LECs, which we termed as ‘initial LECs’ or iLECs, outside the CCV. iLECs emigrated from the CCV as strings of cells and rapidly reorganized into a meshwork. Characteristic changes in cell shape from squamous to spindle shaped, along with the upregulation of Prox1, VEGFR-3 and Nrp2, suggest that LECs upon emigration from the CCV undergo a transition towards a more migratory phenotype. Prox1 has been shown to regulate expression of LEC-specific genes, including VEGFR-3 and Nrp2 (Hong *et al*, 2002; Petrova *et al*, 2002) and VEGFR-3 has been suggested to enhance migration of LECs. Shape change and highly motile behaviour associated with high Prox1 expression have been attributed to a Prox1-mediated upregulation of integrin $\alpha 9 \beta 1$ (Mishima *et al*, 2007), which can also function as a receptor for VEGF-C and D (Vlahakis *et al*, 2005). VEGF-C, probably the most important VEGFR-3 ligand in the context of lymphatic vessel formation, is indispensable for the migration of iLECs. In

VEGF-C-deficient mice, Prox1-expressing LEC progenitors arise but fail to leave the CV (Karkkainen *et al*, 2004). Our results indicate that this is true for all venous vessel beds, and therefore *Vegfc*^{-/-} mice provide an elegant trapping tool to identify venous sources of LEC differentiation. Using this approach, we identified the lower edge of the sVP as a previously unidentified source of LECs. Given the close physical proximity of this structure to the forming PLLV, it is tempting to speculate that parts or even the entire PLLV are derived from iLECs emerging from the sVP, while the pTD is most likely formed by CCV-derived iLECs.

Presently, the analysis of mouse midgestation embryos via ultramicroscopy is limited to fixed samples, which have been chemically cleared to become highly transparent (Mertz, 2011). Therefore, we were not able to dynamically visualize the emerging iLECs. The rapid appearance of massive numbers of iLECs between E10.0 and E10.5 was surprising in view of the comparatively low and constant EdU incorporation of Prox1+ cells between E9.5 and E11.5 (Supplementary Figure 8). Therefore, our analysis is more compatible with a massive and synchronous emigration of iLECs from veins than with high local proliferation and in this respect also argues for additional sources of iLECs besides the CCV. Still the CCV is the first and likely also most important source of iLECs. Furthermore, we conclude from the fact that we were only able to locate Prox1+ cells unequivocally in superficial veins when using mutant *Vegfc*^{-/-} or *Ccbe1*^{-/-} mice that once these cells arise they leave the veins rapidly.

The absence of erythrocytes enclosed by iLECs, but also VE-Cadherin-GFP stainings of cryosections (Supplementary Figure 5G and H), strongly suggested that emerging iLECs are not connected by a patent lumen with the CV. Therefore, our data argue against a separation of LECs from the CV by sprouting. The detection of iLECs was clearly not associated with the appearance of lumenized lymphatic structures contiguous with the CV. In contrast, our analysis, in accord with a most recent publication (Yang *et al*, 2012), supports a model of budding and emigration of individual iLECs from their venous sources.

In this respect, *Ccbe1*^{-/-} embryos behaved remarkably different. Consistent with a recent description (Bos *et al*, 2011), we observed the apparently normal differentiation and accumulation of Prox1+ ECs in the CCV of CCBE1-deficient embryos. Providing new insight into this phenotype and in contrast to wild-type littermates, we detected the appearance of highly irregularly shaped sprouts of Prox1+ ECs from the CV, the ISVs and the endothelium of the sVP. While both mouse strains completely lack iLECs, the aberrant sprout formation clearly distinguished CCBE1 from VEGF-C-deficient mice. In *Ccbe1*^{-/-} embryos, the Prox1 expression domain in the CCV was caudally and cranially extended and now also reached deep into the ISVs. At E10.5, Prox1+ ECs accumulated in the CCV, probably a consequence of their inability to bud. Surprisingly, Prox1 expression was rapidly lost within the next 24 h and subsequently neither detectable in ECs, nor in the developing heart. In contrast, venous EC failed to downmodulate VEGFR-3 expression, which remained unusually high, while numerous aberrant sprouts formed along the entire length of the CV (Figure 7G). During this massive, aberrant sprout formation, VEGFR-3 likely provides and integrates migratory as well as directional cues, while CCBE1 appears



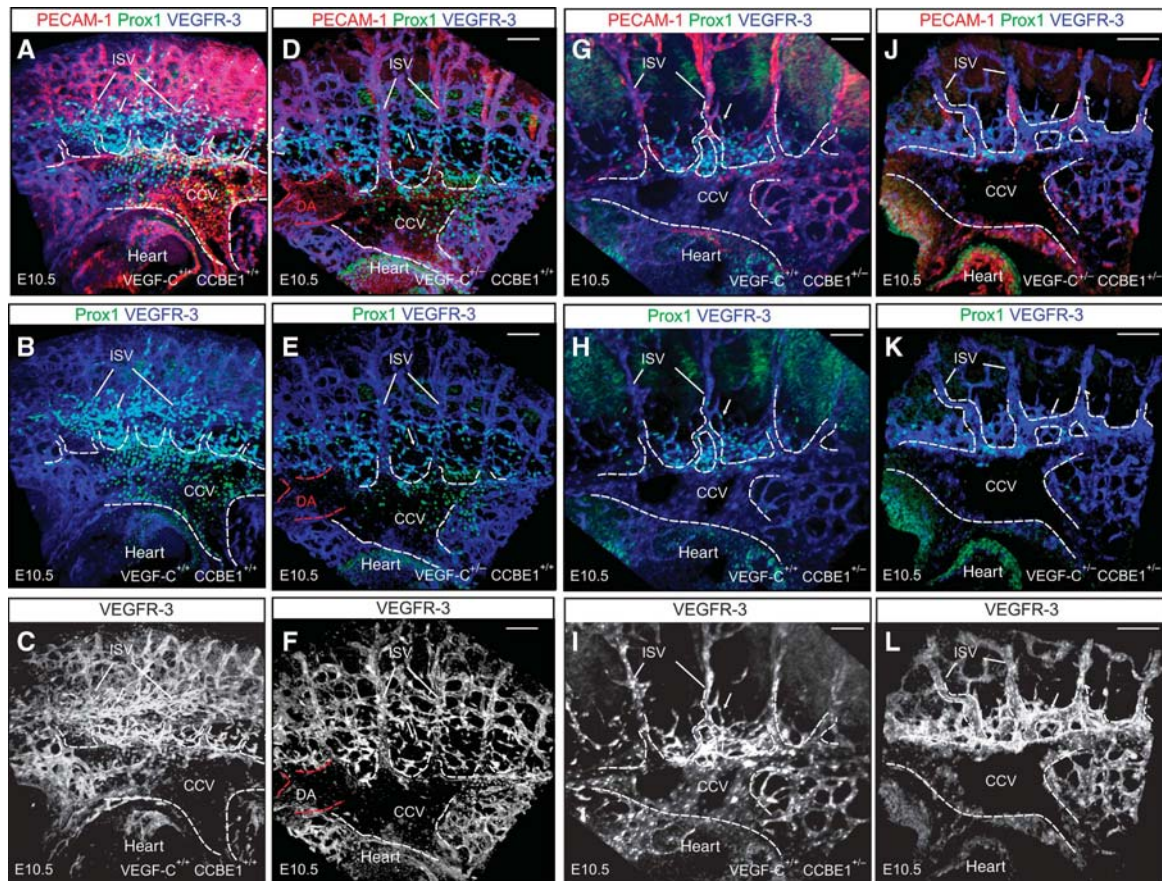


Figure 9 CCBE1 and VEGF-C interact synergistically during iLEC egression and lymph vessel formation. 3D reconstructions of wild-type (A–C), *Vegfc*^{+/-} (D–F), *Ccbe1*^{+/-} (G–I) and *Vegfc*^{+/-}/*Ccbe1*^{+/-} (J–L) embryos, wholemount immunostained for the indicated proteins at E10.5, sagittal view. CCV and roots of the ISVs are indicated by dashed lines, Prox1+ cells by arrows. Compared to wild-type littermates (A–C) *Vegfc*^{+/-} embryos showed a reduction of emigrating iLECs from the CCV (D, E). Contrary to this, in *Ccbe1*^{+/-} embryos an impaired formation of ISVs was detectable. In addition, atypical, lumenized sprouts appeared at the roof of the cardinal vein that were Prox1+ and expressed high levels of VEGFR-3 (G–I). (J–L) In compound heterozygous embryos, this phenotype was grossly exaggerated indicating a synergistic role of VEGF-C and CCBE1 during lymphatic vessel formation. Scale bars = 100 μm.

indispensable for the egress of individual iLECs from the venous cell collective.

Both *Vegfr3* and *Vegfc* heterozygosity most prominently resulted in a reduction of iLECs emerging between the CV and sVP, in accord with the notion that VEGF-C is the predominant VEGFR-3 ligand and VEGFR-3 the most relevant VEGF-C receptor during initial lymphangiogenesis. Somewhat unexpected, we detected malformations of the ISVs and a reduced capacity of iLECs to separate from the CV in *Ccbe1*^{+/-} embryos. These defects are corrected during further development, because analysis of late gestation *Ccbe1*^{+/-} fetuses or neonates revealed no abnormalities. In *Vegfc/Ccbe1* compound heterozygotes, these defects were aggravated demonstrating that both factors synergize during initial lymphangiogenesis.

The exceptional capacity of ultramicroscopy to reveal complex spatial structures enabled us to describe, for the

first time, two separate lymphatic vessels, which have so far been collectively referred to as lymph sacs. Unexpectedly, we detected a first condensation zone of iLECs at the level of the major lateral intersegmental vessel branch, resulting in a lumenized structure that roughly followed the longitudinal axis of the embryo, the PLLV. The PLLV is difficult to spot in histological sections, reiterating the strength of and the need for optical sectioning approaches. A second, large lumenized structure, the pTD, formed more ventrally close to the CV likely by coalescence of lumenized nests of iLEC aggregations. Incorporation of LECs into the pTD was accompanied by a coordinate downregulation of Prox1, VEGFR-3 and *Nrp2*, probably reverting the expression changes that we noted upon egress of iLECs from the CCV.

Junction formation and EC polarization are essential components of vascular lumen formation (Axnick and Lammert, 2012). Several mechanisms of lumen formation have so far

Figure 8 Prox1+ endothelial cells in *VEGF-C*-deficient mouse embryos are unable to leave their vessels of origin and thereby mark the venous sources of LECs. 3D reconstruction of (A, B) wild-type and (C–F) *Vegfc*^{-/-} embryos, wholemount immunostained for the indicated proteins at E10.75, sagittal view. In *VEGF-C*-deficient embryos, Prox1+ endothelial cells were unable to leave venous vessels resulting in an absence of developing lymphatic structures. (E, F) Besides Prox1+ cells in the CV (arrow), a second population of Prox1+ lymphatic progenitors is trapped in a larger venous vessel at the ventral edge of the sVP (arrowhead). (G, H) Schematic representation of Prox1+ cells in wild-type (G) and *VEGF-C*-deficient (H) embryos NE, stripe of neuronal Prox1 expression; sVP, superficial venous plexus, scale bars = 100 μm.

been described including cell hollowing (Kamei *et al*, 2006), chord hollowing (Strilic *et al*, 2009), junctional rearrangement between cells (Blum *et al*, 2008) and selective sprouting (Herbert *et al*, 2009). Our analysis suggests that PLLV and pTD lumen formation is preceded by iLEC aggregation and although loosely reminiscent of chord hollowing, probably different from the mechanisms described for blood vessels. The newly formed lymphatic vessels have a fundamentally different structure compared to the DA and CV. PLLV and pTD are more irregular in shape and of far larger calibre than blood vessels. Therefore, it is likely that additional and unique processes are involved in lumenization following the aggregation of iLECs.

The formation of two initial longitudinal lymphatic vessels bears a distant resemblance to the formation of the zebrafish lymphatic trunk vasculature, where LECs directly bud from the posterior CV. Sprouts that do not connect to primary intersegmental vessels (forming veins in the process), migrate to the horizontal myoseptum where they arrange as a string of parachordal lymphangioblasts (PLs) (Hogan *et al*, 2009; Bussmann *et al*, 2010). Guided by ISAs, PLs then move dorsally and ventrally to form the dorsal longitudinal lymphatic vessel and the TD, which is ventrally located between DA and CV. To which extend these structures are related to the PLLV and pTD remains to be investigated.

A notable exception to the downregulation of Prox1 in large lumenized structures were the contact areas between pTD and CV. High level Prox1 expression has previously been described to be a hallmark and indispensable for lymphovenous valve formation (Srinivasan and Oliver, 2011; Sabine *et al*, 2012). Based on this property, the anatomical position and the frequent occurrence of packed erythrocytes in the pTD close to the contact areas with the CV, we concluded that these sites might give rise to the first lymphovenous valves. The contact sites between pTD and CV always flanked a side branch of the subclavian artery, which crossed the CV at this position. It is an interesting possibility to consider an inductive function of this artery for lymphovenous valve formation. VEGFR-3 heterozygosity apparently did not interfere with ordered lymphovenous valve formation. We should note in this context that our analysis revealed VEGFR-2 expression in the pTD but also weakly in the CV at the time of primordial valve formation (Figure 6I), which might compensate for the loss of VEGFR-3. Interestingly, we had detected robust VEGFR-2 expression earlier in the CV and iLECs.

The axon guidance receptor Unc5B has recently been demonstrated to signal vascular integrity in blood ECs (Koch *et al*, 2011). We found Unc5B expressed on the PLLV, pTD and the newly forming sLECs where it might contribute to structural maintenance during the formation of the lymphatic system. Whether the endothelial-specific Robo family member Robo4, which acts as a counter receptor for Unc5B in blood ECs is expressed in developing LECs remains to be investigated. Interestingly, the canonical Unc5B ligand Netrin-4 was only expressed on the PLLV and pTD. Netrin-4 acts pro-lymphangiogenic, however, these effects are, at least *in vitro*, not mediated by Unc5B, but by the integrin $\alpha 6 \beta 1$ (Larrieu-Lahargue *et al*, 2010, 2011). We found the $\alpha 6$ and $\beta 1$ chains widely expressed on the PLLV, pTD and sLECs, suggesting that integrin $\alpha 6 \beta 1$ is generally of importance for developing LECs. In line with this assumption, integrin $\beta 1$ was recently shown to transduce mechanical forces from

tissue fluid accumulations and to be required for the resulting VEGFR-3 tyrosine phosphorylation, LEC proliferation and lymph vessel expansion (Planas-Paz *et al*, 2012). Being selectively expressed on the PLLV and pTD, Netrin-4 might confer the specific ability for large lumen formation within the newly forming lymphatic system. Whether Unc5B signals via Netrin-4 during lymphatic development remains to be investigated.

In summary, based on optical sectioning microscopy of wholemount immunostained mouse embryos, here we describe in detail structures that have previously collectively been referred to as lymph sacs. We have identified four hallmarks of initial lymphatic vessel formation: (1) iLECs emerge from the roof of the CV, but also from additional venous sources as streams of connected cells, forming a meshwork. (2) iLECs coalesce to lumenized structures at the first lateral intersegmental vessel branch to form the PLLV; sLECs sprouting from the PLLV form dorsal superficial lymphatics. (3) A second large lymphatic structure, the pTD forms from iLEC aggregates close to the CV; lateral sLECs extend from the pTD. (4) Two areas of highest level Prox1 expression demarcate the sites of closest juxtaposition between the CV and pTD and likely give rise to the first lymphovenous valves.

The application of optical sectioning microscopy promises to provide further unexpected insights into the development of vascular structures. An important challenge will be the development of methods to image living embryos and directly observe migrating cell populations.

Materials and methods

Mouse strains

Wild-type, CCBE1^{LacZ/LacZ} (Bos *et al*, 2011), VEGFR-3^{LacZ/LacZ} (Dumont *et al*, 1998) mouse embryos of C57Bl/6 genetic background and VEGF-C^{LacZ/LacZ} (Karkkainen *et al*, 2004) mouse embryos of CD1 background were analysed at different developmental stages between E9.5 and E12.5. Embryonic staging (E) was determined by the day of the vaginal plug (E0.5). All animal experiments were approved by the Animal Experimentation Committee of the county of Münster and the Federal Ministry of Nature, Environment and Consumer Protection, North Rhine Westphalia.

Ultramicroscopy

After immunofluorescence wholemount staining, optically cleared embryos were imaged on a LaVision Ultramicroscope (LaVision BioTec, Bielefeld). Stacks were captured with a step size of 1 μ m and at different magnifications. 3D reconstruction, morphometric analysis and analysis of ultramicroscopy stacks were performed by using IMARIS and IMARIS Vantage software (Version 7.6.0, Bitplane).

Immunofluorescence embryo wholemount stainings

Embryos were dissected and fixed for 4 h in 4% PFA/PBS at 4°C. Prior antibody staining samples were permeabilized (0.5% Triton X-100/PBS) and subsequently blocked in PermBlock solution (1% BSA, 0.5% Tween-20 in PBS). Embryo wholemount stainings were performed by using anti-PECAM-1, anti-VEGFR-3, anti-Prox1, anti-Unc5B and anti-Endomucin as primary antibodies and Alexa-dye coupled secondary antibodies (Invitrogen) diluted in PermBlock. Following each staining step, samples were washed three times in PBS-T (0.5% Tween-20/PBS).

Optical clearing

For visualization, embryo wholemount stainings were embedded in 1% low-melting point agarose. After dehydration in methanol (50%, 70%, 95%, 100%, 100% methanol, each step 30 minutes), samples were twice optically cleared in a benzyl alcohol:benzyl

benzoate solution (ratio 1:2) for 4 h each. Cleared samples were subsequently imaged by ultramicroscopy.

Immunohistochemistry

Embryos were fixed for 4 h in 4% PFA/PBS, washed in PBS, embedded and snap-frozen in OCT. In all, 20 μ m cryo-sections were fixed in ice-cold methanol for 10 min, washed and blocked in PermBlock-3 (3% BSA, 0.5% Tween-20 in PBS). Sections were incubated for 1 h with primary antibodies, washed three times in PBS-T and finally incubated in Alexa-dye conjugated secondary antibodies (Invitrogen). After mounting with mowiol (Calbiochem, 475904), confocal images were captured using a Zeiss LSM 510 meta ($\times 20$, NA=0.8) and Zeiss LSM780 (20x, NA=0.8) confocal microscope.

Antibodies

The following antibodies were used: rabbit polyclonal anti-human Prox1 (ReliaTech, 102-PA30), goat polyclonal anti-human Prox1 (R&D Systems, AF2727), goat polyclonal anti-mouse VEGFR-3 (R&D Systems, AF743), rat monoclonal anti-mouse PECAM-1 (clone 5D2.6 and clone 1G5.1, provided by Dr S Butz), goat polyclonal anti-rat Unc5B (R&D Systems, AF1006), rabbit polyclonal anti-mouse Endomucin (VE44, kindly provided by Prof D Vestweber), hamster monoclonal anti-mouse Podoplanin (clone 8.1.1, in-house made), rat monoclonal anti-human Integrin $\alpha 6$ (GoH3, R&D, MAB13501), rabbit polyclonal anti-mouse Lyve-1 (ReliaTech, 103-PA50), goat polyclonal anti-human Neuropilin-2 (R&D Systems, AF2215), goat polyclonal anti-mouse Netrin-4 (R&D Systems, AF1132), rat monoclonal anti-mouse VEGFR-2 (clone AVAS 12, Biolegend), rat monoclonal anti-mouse Integrin $\beta 1$ (clone MB1.2, Millipore) and rabbit polyclonal anti-GFP (Abcam, ab6556).

Detection of β -galactosidase activity

Embryos between E9.5 and E12.5 were dissected and fixed in a 2% PFA/0.2% glutaraldehyde/PBS solution for 30 min at RT. After washing in PBS, the samples were stained for β -galactosidase activity overnight at 37°C using a β -galactosidase staining kit (Marker Gene Technologies).

Proliferation assay

Proliferation assays were performed using a Click-it EdU Alexa Fluor 647 Proliferation kit (Invitrogen) according to manufacturer's protocol. In brief, pregnant mice were injected with 3.3 mg/kg body weight EdU (5-ethynyl-2'-deoxyuridine). Subsequently, mice were sacrificed and embryos prepared. After fixation, samples were sectioned and histological cryosections were stained with Click-it

EdU detection reagent and vascular markers. EdU-positive cells were visualized using a Zeiss LSM780 ($\times 20$, NA=0.8) confocal microscope.

Statistics

Morphometric analysis of different factors was assessed by quantifying fluorescence intensity in ImageJ with a minimum of $n=20$ different measuring points in each structure. Structures to be compared were always analysed in the same confocal image. The mean of at least $N=3$ different images was calculated and statistically evaluated. Data are presented as mean \pm s.e.m. We analysed data using Mann-Whitney rank-sum test and Student's *t*-test as indicated in the figure legends (Sigma Plot 11.0).

For Imaris Vantage analysis of the nuclear shape: Sphericity Ψ was defined as the ratio of the surface area of a sphere with the same volume as the particle under investigation to the surface area of the particle using the formula $\Psi = \pi^{1/3}(6V_p)^{2/3}/A_p$, with V_p (volume of particle); A_p (surface area of particle). Ellipticity e was defined as the pointedness of a prolate spheroid, that is, one for which the polar radius (c) is greater than the equatorial radius (a) $e = \sqrt{c^2 - a^2}/c$.

Supplementary data

Supplementary data are available at *The EMBO Journal* Online (<http://www.embojournal.org>).

Acknowledgements

We thank Dietmar Vestweber and Wiebke Herzog for critically reviewing and discussing the manuscript, Ludmila Kremer and Nannette Kumpel-Rink for expert in-house transgenic services, and Uwe Schröer for technical support. This work was supported in part by grants from the Deutsche Forschungsgemeinschaft (SFB 629, SFB 656) and the Max-Planck-Society to FK.

Author contributions: FK conceived the project, designed experiments, analysed data and wrote the manuscript; RH and CP designed and performed experiments, analysed and interpreted data and contributed to the manuscript; MA and CS performed and analysed experiments; VA provided valuable help with ultramicroscopy and contributed to the manuscript, HN, RA and KA provided reagents. SS-M provided reagents and contributed to the manuscript.

Conflict of interest

The authors declare that they have no conflict of interest.

References

- Abtahian F, Guerriero A, Sebзда E, Lu MM, Zhou R, Mocsai A, Myers EE, Huang B, Jackson DG, Ferrari VA, Tybulewicz V, Lowell CA, Lepore JJ, Koretzky GA, Kahn ML (2003) Regulation of blood and lymphatic vascular separation by signaling proteins SLP-76 and Syk. *Science* **299**: 247–251
- Adams RH, Eichmann A (2010) Axon guidance molecules in vascular patterning. *Cold Spring Harb Perspect Biol* **2**: a001875
- Axnck J, Lammert E (2012) Vascular lumen formation. *Curr Opin Hematol* **19**: 192–198
- Becker K, Jahrling N, Kramer ER, Schnorrer F, Dodt HU (2008) Ultramicroscopy: 3D reconstruction of large microscopical specimens. *J Biophotonics* **1**: 36–42
- Blum Y, Belting HG, Ellertsdottir E, Herwig L, Luders F, Affolter M (2008) Complex cell rearrangements during intersegmental vessel sprouting and vessel fusion in the zebrafish embryo. *Dev Biol* **316**: 312–322
- Bohmer R, Neuhaus B, Buhren S, Zhang D, Stehling M, Bock B, Kiefer F (2010) Regulation of developmental lymphangiogenesis by Syk(+) leukocytes. *Dev Cell* **18**: 437–449
- Bos FL, Caunt M, Peterson-Maduro J, Planas-Paz L, Kowalski J, Karpanen T, van IA, Tong R, Ernst JA, Korving J, van Es JH, Lammert E, Duckers HJ, Schulte-Merker S (2011) CCBE1 is essential for mammalian lymphatic vascular development and enhances the lymphangiogenic effect of vascular endothelial growth factor-C in vivo. *Circ Res* **109**: 486–491
- Bussmann J, Bos FL, Urasaki A, Kawakami K, Duckers HJ, Schulte-Merker S (2010) Arteries provide essential guidance cues for lymphatic endothelial cells in the zebrafish trunk. *Development* **137**: 2653–2657
- D'Amico G, Alitalo K (2010) Inside bloody lymphatics. *Blood* **116**: 512–513
- Dumont DJ, Jussila L, Taipale J, Lymboussaki A, Mustonen T, Pajusola K, Breitman M, Alitalo K (1998) Cardiovascular failure in mouse embryos deficient in VEGF receptor-3. *Science* **282**: 946–949
- Francois M, Caprini A, Hosking B, Orsenigo F, Wilhelm D, Browne C, Paavonen K, Karnezis T, Shayan R, Downes M, Davidson T, Tutt D, Cheah KS, Stacker SA, Muscat GE, Achen MG, Dejana E, Koopman P (2008) Sox18 induces development of the lymphatic vasculature in mice. *Nature* **456**: 643–647
- Francois M, Short K, Secker GA, Combes A, Schwarz Q, Davidson TL, Smyth I, Hong YK, Harvey NL, Koopman P (2012) Segmental territories along the cardinal veins generate lymph sacs via a ballooning mechanism during embryonic lymphangiogenesis in mice. *Dev Biol* **364**: 89–98
- Fu J, Gerhardt H, McDaniel JM, Xia B, Liu X, Ivanciu L, Ny A, Hermans K, Silasi-Mansat R, McGee S, Nye E, Ju T, Ramirez MI, Carmeliet P, Cummings RD, Lupu F, Xia L (2008) Endothelial cell

- O-glycan deficiency causes blood/lymphatic misconnections and consequent fatty liver disease in mice. *J Clin Invest* **118**: 3725–3737
- Herbert SP, Huisken J, Kim TN, Feldman ME, Houseman BT, Wang RA, Shokat KM, Stainier DY (2009) Arterial-venous segregation by selective cell sprouting: an alternative mode of blood vessel formation. *Science* **326**: 294–298
- Hogan BM, Bos FL, Bussmann J, Witte M, Chi NC, Duckers HJ, Schulte-Merker S (2009) Ccbe1 is required for embryonic lymphangiogenesis and venous sprouting. *Nat Genet* **41**: 396–398
- Hong YK, Harvey N, Noh YH, Schacht V, Hirakawa S, Detmar M, Oliver G (2002) Prox1 is a master control gene in the program specifying lymphatic endothelial cell fate. *Dev Dyn* **225**: 351–357
- Kaipainen A, Korhonen J, Mustonen T, van Hinsbergh VW, Fang GH, Dumont D, Breitman M, Alitalo K (1995) Expression of the fms-like tyrosine kinase 4 gene becomes restricted to lymphatic endothelium during development. *Proc Natl Acad Sci USA* **92**: 3566–3570
- Kamei M, Saunders WB, Bayless KJ, Dye L, Davis GE, Weinstein BM (2006) Endothelial tubes assemble from intracellular vacuoles in vivo. *Nature* **442**: 453–456
- Karkkainen MJ, Haiko P, Sainio K, Partanen J, Taipale J, Petrova TV, Jeltsch M, Jackson DG, Talikka M, Rauvala H, Betscholtz C, Alitalo K (2004) Vascular endothelial growth factor C is required for sprouting of the first lymphatic vessels from embryonic veins. *Nat Immunol* **5**: 74–80
- Karpanen T, Heckman CA, Keskkitalo S, Jeltsch M, Ollila H, Neufeld G, Tamagnone L, Alitalo K (2006) Functional interaction of VEGF-C and VEGF-D with neuropilin receptors. *FASEB J* **20**: 1462–1472
- Kim H, Koh GY (2010) Platelets take the lead in lymphatic separation. *Circ Res* **106**: 1184–1186
- Koch AW, Mathivet T, Larrivee B, Tong RK, Kowalski J, Pibouin-Fragner L, Bouvree K, Stawicki S, Nicholes K, Rathore N, Scales SJ, Luis E, del TR, Freitas C, Breant C, Michaud A, Corvol P, Thomas JL, Wu Y, Peale F *et al* (2011) Robo4 maintains vessel integrity and inhibits angiogenesis by interacting with UNC5B. *Dev Cell* **20**: 33–46
- Larrieu-Lahargue F, Welm AL, Thomas KR, Li DY (2010) Netrin-4 induces lymphangiogenesis in vivo. *Blood* **115**: 5418–5426
- Larrieu-Lahargue F, Welm AL, Thomas KR, Li DY (2011) Netrin-4 activates endothelial integrin $\alpha_6\beta_1$. *Circ Res* **109**: 770–774
- Mertz J (2011) Optical sectioning microscopy with planar or structured illumination. *Nat Methods* **8**: 811–819
- Mishima K, Watabe T, Saito A, Yoshimatsu Y, Imaizumi N, Masui S, Hirashima M, Morisada T, Oike Y, Araie M, Niwa H, Kubo H, Suda T, Miyazono K (2007) Prox1 induces lymphatic endothelial differentiation via integrin α_9 and other signaling cascades. *Mol Biol Cell* **18**: 1421–1429
- Norrmen C, Ivanov KI, Cheng J, Zangger N, Delorenzi M, Jaquet M, Miura N, Puolakkainen P, Horsley V, Hu J, Augustin HG, Yla-Herttuala S, Alitalo K, Petrova TV (2009) FOXC2 controls formation and maturation of lymphatic collecting vessels through cooperation with NFATc1. *J Cell Biol* **185**: 439–457
- Oliver G (2004) Lymphatic vasculature development. *Nat Rev Immunol* **4**: 35–45
- Petrova TV, Makinen T, Makela TP, Saarela J, Virtanen I, Ferrell RE, Finegold DN, Kerjaschki D, Yla-Herttuala S, Alitalo K (2002) Lymphatic endothelial reprogramming of vascular endothelial cells by the Prox-1 homeobox transcription factor. *EMBO J* **21**: 4593–4599
- Planas-Paz L, Strlic B, Goedecke A, Breier G, Fassler R, Lammert E (2012) Mechanoinduction of lymph vessel expansion. *EMBO J* **31**: 788–804
- Sabin FR (1902) On the origin of the lymphatic system from the veins and the development of the lymph hearts and thoracic duct in the pig. *Am J Anat* **1**: 367–389
- Sabine A, Agalarov Y, Maby-El HH, Jaquet M, Hagerling R, Pollmann C, Beber D, Pfenniger A, Miura N, Dormond O, Calmes JM, Adams RH, Makinen T, Kiefer F, Kwak BR, Petrova TV (2012) Mechanotransduction, PROX1, and FOXC2 cooperate to control connexin37 and calcineurin during lymphatic-valve formation. *Dev Cell* **22**: 430–445
- Schacht V, Ramirez MI, Hong YK, Hirakawa S, Feng D, Harvey N, Williams M, Dvorak AM, Dvorak HF, Oliver G, Detmar M (2003) T1alpha/podoplanin deficiency disrupts normal lymphatic vasculature formation and causes lymphedema. *EMBO J* **22**: 3546–3556
- Schulte-Merker S, Sabine A, Petrova TV (2011) Lymphatic vascular morphogenesis in development, physiology, and disease. *J Cell Biol* **193**: 607–618
- Srinivasan RS, Dillard ME, Lagutin OV, Lin FJ, Tsai S, Tsai MJ, Samokhvalov IM, Oliver G (2007) Lineage tracing demonstrates the venous origin of the mammalian lymphatic vasculature. *Genes Dev* **21**: 2422–2432
- Srinivasan RS, Oliver G (2011) Prox1 dosage controls the number of lymphatic endothelial cell progenitors and the formation of the lymphovenous valves. *Genes Dev* **25**: 2187–2197
- Strlic B, Kucera T, Eglinger J, Hughes MR, McNagny KM, Tsukita S, Dejana E, Ferrara N, Lammert E (2009) The molecular basis of vascular lumen formation in the developing mouse aorta. *Dev Cell* **17**: 505–515
- Suzuki-Inoue K, Kato Y, Inoue O, Kaneko MK, Mishima K, Yatomi Y, Yamazaki Y, Narimatsu H, Ozaki Y (2007) Involvement of the snake toxin receptor CLEC-2, in podoplanin-mediated platelet activation, by cancer cells. *J Biol Chem* **282**: 25993–26001
- Tammela T, Alitalo K (2010) Lymphangiogenesis: Molecular mechanisms and future promise. *Cell* **140**: 460–476
- Tammela T, Zarkada G, Wallgard E, Murtomaki A, Suchting S, Wirzenius M, Waltari M, Hellstrom M, Schomber T, Peltonen R, Freitas C, Duarte A, Isoniemi H, Laakkonen P, Christofori G, Yla-Herttuala S, Shibuya M, Pytowski B, Eichmann A, Betscholtz C *et al* (2008) Blocking VEGFR-3 suppresses angiogenic sprouting and vascular network formation. *Nature* **454**: 656–660
- Uhrin P, Zaujec J, Breuss JM, Olcaydu D, Chrenek P, Stockinger H, Fuertbauer E, Moser M, Haiko P, Fassler R, Alitalo K, Binder BR, Kerjaschki D (2010) Novel function for blood platelets and podoplanin in developmental separation of blood and lymphatic circulation. *Blood* **115**: 3997–4005
- Vlahakis NE, Young BA, Atakilit A, Sheppard D (2005) The lymphangiogenic vascular endothelial growth factors VEGF-C and -D are ligands for the integrin $\alpha_9\beta_1$. *J Biol Chem* **280**: 4544–4552
- Wigle JT, Harvey N, Detmar M, Lagutina I, Grosveld G, Gunn MD, Jackson DG, Oliver G (2002) An essential role for Prox1 in the induction of the lymphatic endothelial cell phenotype. *EMBO J* **21**: 1505–1513
- Wigle JT, Oliver G (1999) Prox1 function is required for the development of the murine lymphatic system. *Cell* **98**: 769–778
- Yang Y, Garcia-Verdugo JM, Soriano-Navarro M, Srinivasan RS, Scallan JP, Singh MK, Epstein JA, Oliver G (2012) Lymphatic endothelial progenitors bud from the cardinal vein and intersomitic vessels in mammalian embryos. *Blood* **120**: 2340–2348



The EMBO Journal is published by Nature Publishing Group on behalf of European Molecular Biology Organization. This article is licensed under a Creative Commons Attribution-NonCommercial-Share Alike 3.0 Licence. [<http://creativecommons.org/licenses/by-nc-sa/3.0/>]